INL/MIS-20-61167-Revision-0

Mesoscale simulations of High Burnup Fuel Fragmentation

December 2020

Larry K Aagesen Jr, Sudipta Biswas, Wen Jiang, Kyle A Gamble

Changing the World's Energy Future

Idaho National Laboratory

INL is a U.S. Department of Energy National Laboratory operated by Battelle Energy Alliance, LLC

INL/MIS-20-61167-Revision-0

Mesoscale simulations of High Burnup Fuel Fragmentation

Larry K Aagesen Jr, Sudipta Biswas, Wen Jiang, Kyle A Gamble

December 2020

Idaho National Laboratory
Idaho Falls, Idaho 83415

http://www.inl.gov

Prepared for the
U.S. Department of Energy
Under DOE Idaho Operations Office
Contract DE-AC07-05ID14517

Mesoscale simulations of High Burnup Fuel Fragmentation

Applying phase-field modeling to understand high burnup fuel fragmentation during loss of coolant accident conditions

InsertSAPNumberHere

Final Report, December 2020

EPRI Project Manager

R. Daum

DISCLAIMER OF WARRANTIES AND LIMITATION OF LIABILITIES

INSERT APPROPRIATE AUTO TEXT DISCLAIMER HERE.

NOTE

For further information about EPRI, call the EPRI Customer Assistance Center at 800.313.3774 or e-mail askepri@epri.com.

ACKNOWLEDGMENTS

The following organizations, under contract to the Electric Power Research Institute (EPRI), prepared this report:

Idaho National Laboratory
P. O. Box 1625
Idaho Falls, ID 83415

Principal Investigator
L. Aagesen

Other Participants
S. Biswas, K. Gamble, W. Jiang

This report describes research sponsored by EPRI.

This publication is a corporate document that should be cited in the literature in the following manner:

Mesoscale simulations of High Burnup Fuel Fragmentation: Applying phase-field modeling to understand high burnup fuel fragmentation during loss of coolant accident conditions. EPRI, Palo Alto, CA: 2020. InsertSAPNumberHere.

ABSTRACT

During a loss-of-coolant accident (LOCA) in a nuclear power plant, a rapid increase in temperature is experienced in the fuel. In commercial light water reactors (LWRs), the high burnup structure (HBS) forms in regions of the UO_2 fuel where local burnup is high, characterized by smaller grain sizes and large, overpressurized bubbles. During a LOCA transient, fuel in the HBS region is susceptible to fine fragmentation, where the fuel breaks up into micron-size fragments (sometimes referred to as pulverization). To better understand the mechanisms behind this phenomenon, mesoscale computational modeling using the Idaho National Laboratory code Marmot has been employed to simulate the process of HBS formation and response to a LOCA transient. The process of complete and partial HBS formation was demonstrated in prototypical LWR conditions. The simulated HBS microstructures from these simulations were passed to a phase-field model of fracture. To provide a more direct comparison with experiments, a set of experiments conducted by Studsvik on fine fragmentation/pulverization during LOCA conditions was simulated using the BISON fuel performance code. The temperature profiles from the BISON simulations were passed to a phase-field model to determine the gas bubble pressure as a function of time. These pressure histories were used in a phase-field model of fracture to determine under what conditions and in which types of bubbles fine fragmentation was likely to occur.

Keywords

Fragmentation, pulverization, LOCA, phase-field, HBS, fracture

Deliverable Number: InsertSAPNumberHere

Product Type: Technical Report

Product Title: Mesoscale simulations of High Burnup Fuel Fragmentation: Applying phase-field modeling to understand high burnup fuel fragmentation during loss of coolant accident conditions

---

PRIMARY AUDIENCE: Commercial fuel developers and nuclear utilities

SECONDARY AUDIENCE: Scientists and engineers studying nuclear fuel behavior

KEY RESEARCH QUESTION

To improve the financial performance of existing nuclear power plants, nuclear utilities are currently seeking to obtain approval for increased burnup limits for UO_2 fuel. A key safety concern in such an increase in burnup limits is the potential for fine fragmentation/pulverization during a loss of coolant accident (LOCA), which predominantly occurs in regions of the fuel where the high burnup structure (HBS) has partially or completely formed. If a cladding rupture occurs simultaneously during the LOCA, these fine fragments of fuel can be carried out of the core by the coolant. However, the mechanism by which fine fragmentation/pulverization occurs is not well understood. The purpose of this work is to develop an improved mechanistic understanding of fine fragmentation/pulverization at the microstructural level and to aid in developing and parameterizing an engineering-scale model of fine fragmentation/pulverization in the BISON fuel performance code.

RESEARCH OVERVIEW

Meso-scale computational modeling (using the phase-field method as implemented in the code Idaho National Laboratory code Marmot) was employed to study the formation of the high burnup structure, in cases where both partial and complete HBS formation occurred. The simulated HBS microstructures were analyzed and were also passed into a phase-field model of fracture to investigate the effect of microstructure on fracture behavior, particularly in regions where only partial HBS formation has occurred. An experiment conducted by Studsvik that aimed to replicate LOCA conditions was simulated using the BISON fuel performance code, and the temperature history from these simulations was used as input to a phase-field model of bubble pressure response. From this model, the pressure history was passed to a phase-field fracture model. The conditions leading to fine fragmentation were investigated using this model.

KEY FINDINGS

- The recrystallization initiates at the grain boundaries and proceeds inwards towards the grain interiors
- At low temperature, continuous grain subdivision takes place, whereas with higher temperature grain nucleation is followed by a coarsening stage
- During LOCA transients, the sizes of bubbles in the HBS region did not change significantly.
- The pressurized bubble can cause cracks initiation and propagation. The size of the bubble and external pressure will change the critical pressure for crack initiation. Multiple bubbles can form fragmentations through cracks propagation, and their spatial distribution can change the size and shape of fragmentations.

WHY THIS MATTERS

Improved mechanistic understanding of fine fragmentation/pulverization will contribute to the development of a mechanistic model of the process, which will be implemented in the BISON nuclear fuel performance code. Use of this code will aid nuclear utilities and fuel developers in making a better-informed case for increasing burnup limits, the approval of which will improve financial performance of the plants.

EPRI | ELECTRIC POWER RESEARCH INSTITUTE

EXECUTIVE SUMMARY

HOW TO APPLY RESULTS

Stakeholders interested in gaining access to the BISON nuclear fuel performance code can apply to obtain access at the website bison.inl.gov. The mesoscale simulation code Marmot used to conduct the simulations in this report can also be licensed to interested parties through the website moose.inl.gov/marmot.

LEARNING AND ENGAGEMENT OPPORTUNITIES

- The research conducted here has been performed collaboratively with the Department of Energy's NEAMS (Nuclear Energy Advanced Modeling and Simulation) program, which provided funding for development of the software codes used. It is expected that these results will be used in the program's efforts to develop a microstructure-informed model for fine fragmentation/pulverization in the BISON code.

EPRI CONTACTS: Rob Daum, rdaum@epri.com

PROGRAM: Add Program Name and Number here.

IMPLEMENTATION CATEGORY: Add Nuclear Product Implementation Category here.

Electric Power Research Institute
3420 Hillview Avenue, Palo Alto, California 94304-1338 • PO Box 10412, Palo Alto, California 94303-0813 USA
800.313.3774 • 650.855.2121 • askepri@epri.com • www.epri.com

CONTENTS

LIST OF FIGURES

Insert LOF Macro Here

LIST OF TABLES

Insert LOT Macro Here

1 INTRODUCTION

In order to improve the economics of commercial nuclear energy production, U.S. fuel vendors and utilities are currently seeking to increase the burnup limit of pellet-form UO_2 fuel for commercial light water reactors (LWRs) from 62 GWd/MTU to as high as 75 GWd/MTU [1]. To gain approval for such an increase, vendors must demonstrate that fuel rods remain safe for design basis accidents. One significant challenge in increasing the burnup limit is demonstrating safety in the case of a Loss of Coolant Accident (LOCA). During a LOCA, the fuel can fragment into very small pieces (sometimes referred to as pulverization) [2,3]. In the event of a rupture of the cladding during the LOCA, these small fragments (with diameters of less than 100 μm [4]) could escape to the coolant. To allow fuel to be used to higher burnups, the cause of this pulverization phenomena must be better understood and mitigation strategies must be developed.

Although the cause of pulverization is not fully understood, it has been linked with the formation of the high burnup structure (HBS) in UO_2 [4]. The formation of the HBS is itself not fully understood, but it results in two main changes in the fuel microstructure. The first is the formation of a finer grain structure through a process of recrystallization or polygonization [5]. This results in a decrease in grain size of from typical as-fabricated grain sizes of 5 to 10 μm to much smaller sizes of 100-300 nm. At the same time, larger fission gas bubbles form with diameters in the range of 1 μm, with many of the new, smaller grains intersecting each bubble. These larger bubbles are believed to be significantly overpressurized with fission gases relative to the equilibrium pressure predicted by the Gibbs-Thomson condition [6]. At the same time, fission gas is depleted in the fuel matrix surrounding the bubbles.

Pulverization has predominantly been observed in regions where either partial or complete HBS formation has occurred [4]. During a LOCA transient, a rapid increase in temperature occurs, causing an increase in pressure in the already overpressurized bubbles in the HBS region. It has been hypothesized that this rapid increase in pressure causes fracture along the grain or subgrain boundaries that intersect the large bubbles in the HBS region, leading to fine fragmentation. Although the mechanism of pulverization is not fully understood, because of its importance to fuel performance, an empirical criterion for pulverization has been implemented in BISON based on experimental data [4]. However, to provide predictive capability outside the conditions in which these experiments were conducted, a mechanistic criterion for pulverization that accounts for the microstructure of the fuel is desired.

In this work, mesoscale simulations are employed to provide insight into the formation of the HBS and to investigate the effects of LOCA-type temperature transients on fuel with this microstructure. These simulations provide a basis for development of a mechanistic pulverization criterion for BISON. The simulations conducted in this work make use of mesoscale models developed in the phase-field code Marmot through the NEAMS program. Details of the phase-field models are described elsewhere [7]. In Section 2, a phase-field model of HBS formation is

used to study partial and complete HBS formation, and provide input of representative microstructures for further simulations using a phase-field fracture model. This model tracks U-site vacancies and gas atoms and includes their production with source terms. Recrystallization is included in the model through the formation of new grains when the local dislocation density exceeds a critical value. In Section 3, the effect of LOCA-type temperature transients on large fission gas bubbles in the HBS region is investigated. A set of experiments conducted by Studsvik on fine fragmentation/pulverization during LOCA-type conditions was simulated using the BISON fuel performance code. The temperature profiles from the BISON simulations were passed to a phase-field model to determine the gas bubble pressure as a function of time. No significant change in bubble size occurs as a result of the temperature transient. The gas pressure during the transient is also calculated as a function of time and passed to the phase field model of fracture. In Section 4, a phase-field fracture model is used that includes the effect of pressure in the bubble that propagates along newly formed cracks that intersect the bubble. Simulations using the model show that fracture occurs along grain boundaries surrounding the large fission gas bubbles due to the pressure in the bubble, in agreement with the hypothesized mechanism of pulverization during LOCA transients.

References

1. F. Pimentel and F. Smith. The economic benefits and challenges with utilizing increased enrichment and fuel burnup for light-water reactors. Technical report, Nuclear Energy Institute, 2019.

2. M. Helin and J. Flygare. NRC LOCA tests at Studsvik, design and construction of test train device and tests with unirradiated cladding material. Technical Report, STUDSVIK/N-11/130, Studsvik, 2012.

3. M. Flanagan and P. Askeljung. Observations of fuel fragmentation, mobility and release in integral high-burnup, fueled LOCA tests. In *Enlarged Halden Program Group Meeting 2011*, 2011.

4. J. A. Turnbull, S. K. Yagnik, M. Hirai, D. M. Staicu, and C. T. Walker. An assessment of the fuel pulverization threshold during LOCA-type temperature transients. *Nuclear Science and Engineering*, 179:477–485, 2015.

5. V. V. Rondinella and T. Wiss. The high burn-up structure in nuclear fuel. *Materials Today*, 13:24–32, 2010.

6. K. Nogita and K. Une. Irradiation-induced recrystallization in high burnup UO_2 fuel. *Journal of Nuclear Materials*, 226(3):302–310, 1995.

7. L. K. Aagesen, S. Biswas, W. Jiang, A. M. Jokisaari, D. Andersson, M. W. D. Cooper, C. Matthews. Determine fragmentation criteria in high-burnup UO_2 fuel during accident conditions. Technical report, INL/EXT-20-00558, Idaho National Laboratory, 2020.

2
HIGH BURNUP STRUCTURE FORMATION

In UO_2 fuel, regions exposed to high burn-up and low temperatures exhibit a fine-grained microstructure with large bubbles known as high burn-up structure (HBS). The key characteristics of the region include a) accumulation of dislocations leading to creation of large dislocation networks, b) recrystallization of new defect free sub-grains, c) depletion of intra-granular fission gas concentration, and d) formation of large spherical inter-granular bubbles [1]. Understanding the HBS formation and its impact on the thermo-mechanical properties of the nuclear fuel is very important to evaluate the performance of the fuel, especially in accident scenarios.

In this section, the high burnup structure creation is demonstrated using a phase-field model. The model employs a dislocation density based discrete nucleation algorithm to capture the formation of smaller grains via recrystallization, due to defect accumulation over time. The model also accounts for existing fission gas bubbles and concurrently tracks the concentration of defects, such as vacancies and gas atoms. The details about the model and can be found in [2]. The model is capable of generating realistic HBS including the partially restructured ones, similar to what has been observed experimentally [3]. The microstructures generated from these simulations can be utilized to evaluate the effect of the structure on the thermo-mechanical properties and fragmentation of the fuel.

For the demonstration, a 12.5 μm × 12.5 μm simulation domain with four large grains and a bubble with 1.2 μm radius is chosen. The grains are initialized with randomly generated dislocation densities with values representing irradiated fuel. The defect source terms are defined based on a typical LWR fission rate of 1×10^{19} fission/m^3/s. A time dependent burnup increase is considered, and the associated dislocation density is calculated based on the effective burnup using the correlation proposed in [4]. The effective burnup for a grain is calculated based on a linear burnup increase with time starting from the time the grain is created. For computational benefits, MOOSE and its grain tracker algorithm [5] is used. In this section, we present the HBS formation at 1000 K and 1100 K temperatures.

Figure 2.1 shows different stages of HBS formation at 1000 K temperature along with the corresponding recrystallization fraction. Here, the recrystallization fraction is defined as the fraction of the domain covered by the newly formed grains. As observed in Figure 1, the grain nucleation initiates at the grain boundaries and the bubble/grain interfaces. Subsequently, it proceeds inward towards the grain interior, eventually engulfing the whole grain. Here, the partially recrystallized structure is identified by the retention of the initial grain structures while the grain refinement continues. Due to low grain boundary mobility, there is no significant grain growth at this temperature. At the end of complete restructuring, the domain includes 1528 grains with average grain radius of 168 nm. It is noteworthy here that due to the damage accumulation in the earlier recrystallized grains, grain subdivision continues even after the original structure is completely destructed.

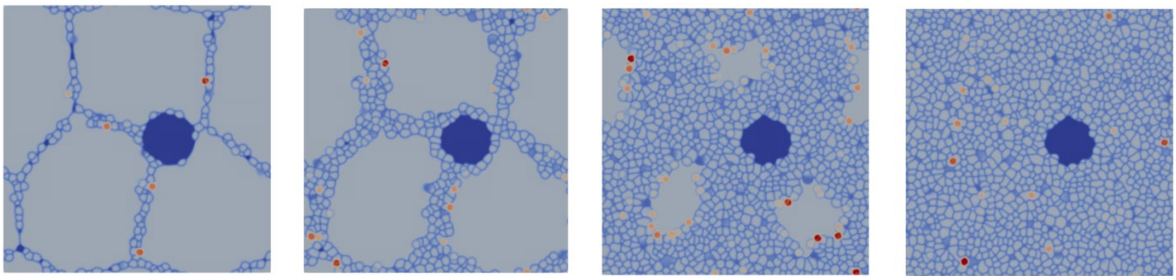

(a) (b) (c) (d)

Figure 2.1. HBS formation at 1000 K a) 12.84% recrystallized grains at 1.19×10^6 sec, b) 30.33% recrystallized grains at 2.78×10^6 sec, c) 85.76% recrystallized grains at 3.67×10^6 sec, c) 100% recrystallized grains at 3.97×10^6 sec. Light blue lines indicate grain boundaries, dark blue region is the bubble, gray area is within a grain, and red denotes the most recent grain nucleation.

The ability of the model to retain initial grain structures even as the new damage free grains are created is further illustrated by Fig. 2.2. Here, the dislocation density (Figure 2.2a) and the effective burnup (Figure 2.2b) is plotted for the 85.76% recrystallized structure (the red zones indicate the initial damaged grains). It shows that the initial damaged grains are exposed to higher effective burnup and has higher dislocation density compared to the recrystallized grains. The newly formed grains are considered defect free as indicated by low burnup and dislocations density. It also exhibits that the grains created at the earlier stage of restructuring accumulate burnup as well as defects over time due to their exposure to irradiation. This leads to further restructuring of the HBS in stages.

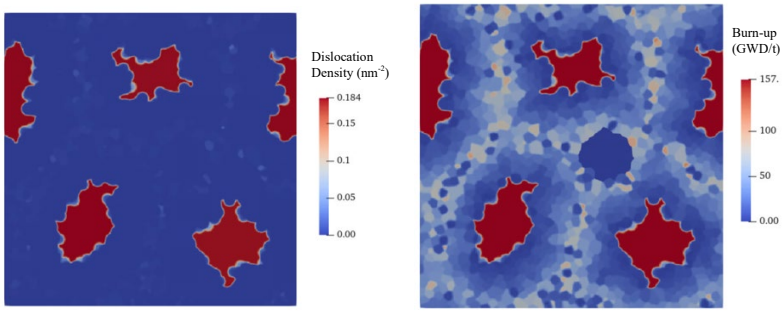

(a) (b)

Figure 2.2 Demonstration of partial recrystallization for 85.76 % recrystallized structure with a) dislocation density variation, and b) effective burnup accumulation. Red zones indicate preexisting damaged grains.

Next, the HBS formation is studied at 1100 K temperature. Figure 2.3 represents different stages of HBS formation at 1100 K along with the corresponding recrystallization fraction. In this case, grain nucleation is followed by a grain growth stage where the larger grains grow at the expense of the smaller ones. At this stage, there is a competition between coarsening of previously formed

grains and stabilization of the newly nucleated ones. However, as time progresses, the dislocation density keeps increasing and the restructuring continues. At the end of the first stage of complete restructuring, the domain includes 215 grains with average grain radius of 396 nm. The partially recrystallized structures obtained from this simulation has been provided as an input structure for the mesoscale fracture simulations.

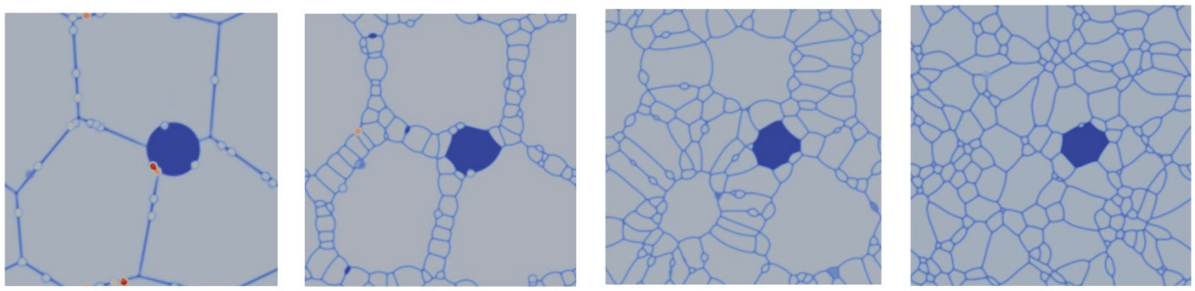

(a) (b) (c) (d)

Figure 2.3. HBS formation at 1100 K a) starting of recrystallization, b) 25.17% recrystallized grains at 7.94×10^5 sec, c) 60.34% recrystallized grains at 2.24×10^6 sec, and d) 100% recrystallized grain at 2.83×10^6 sec. Light blue lines indicates grain boundaries, dark blue region is bubble, gray area is within a grain, and red denotes the most recent grain nucleation.

Figure 2.4 compares the grain statistics during the restructuring process at 1000 K and 1100 K temperatures. At 1000 K, the grain nucleation occurs at a steady rate without significant grain growth. As a result, the number of grains constantly rises, and the average grain radius decreases. On the other hand, at 1100 K, the restructuring follows a seesaw pattern where the grain nucleation is succeeded by a grain growth stage. During the nucleation stage, no. of grains sharply increases, and average grain radius decreases. During the subsequent growth stage, the number of grains slowly decreases, as the coarsening prevails over the stabilization of the newly nucleated grains. Two distinct nucleation peaks are witnessed in this case.

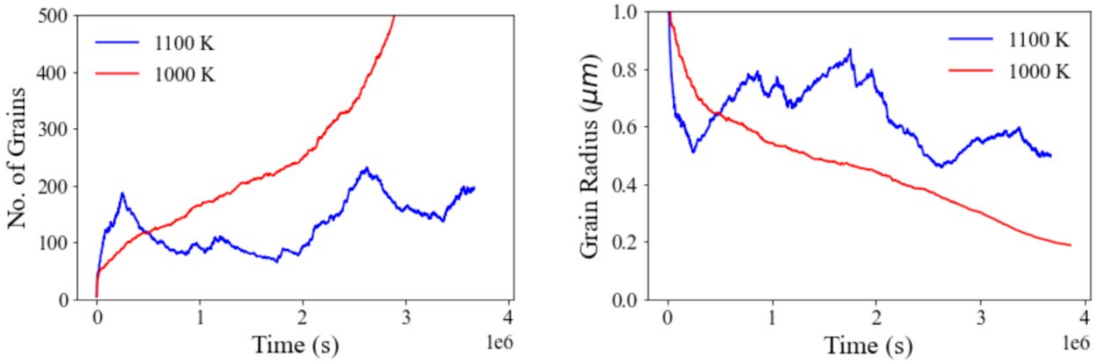

(a) (b)

Figure 2.4. Grain statistics over time demonstrating a) no. of grain variation, and b) average grain radius variation.

The mesoscale simulation provides some important insights towards understanding the restructuring process leading to HBS formation. It also generates microstructures that can be used for property and performance evaluation of the fuel. Microstructures at different stages of HBS formation can be used as an input structure for meso-scale fragmentation analysis. For the simulations presented in this section, bubble growth was not observed during the restructuring. It was previously demonstrated that the growth of the large bubbles is facilitated after the completion of recrystallization [2]. Consideration of various defects and their recombination is required to make the model more predictive for bubble growth. Moreover, further analysis is required to understand the bubble gas pressure buildup during the process. Inclusion of a mechanistic dislocation density calculation would also increase the accuracy of the model. Finally, 3D analysis could potentially provide better understanding about the bubble evolution in HBS.

References

1. Vincenzo V. Rondinella and Thierry Wiss. The high burn-up structure in nuclear fuel. Materials Today, 13(12):24-32, 2010.

2. L. K. Aagesen, S. Biswas, W. Jiang, A. M. Jokisaari, D. Andersson, M. W. D. Cooper, C. Matthews. Determine fragmentation criteria in high-burnup UO_2 fuel during accident conditions. Technical report, INL/EXT-20-00558, Idaho National Laboratory, 2020.

3. Tyler J. Gerczak, Chad M. Parish, Philip D. Edmondson, Charles A. Baldwin, Kurt A. Terrani. Restructuring in high burnup UO2 studied using modern electron microscopy. Journal of Nuclear Materials, 509: 245-259, 2018.

4. K. Nogita and K. Une. Irradiation-induced recrystallization in high burnup UO_2 fuel. *Journal of Nuclear Materials*, 226(3):302–310, 1995.

5. C. J. Permann, M. R. Tonks, B. Fromm, and D. R. Gaston. Order parameter re-mapping algorithm for 3D phase field model of grain growth using FEM. Computational Materials Science, 115:18–25, 2016.

3
MODELING OF HIGH BURNUP STRUCTURE BUBBLE RESPONSE TO LOCA TRANSIENTS

Within the region where the HBS has formed, fission gas bubbles are relatively large, with diameters on the order of 1 micron. It is also believed that the bubbles are overpressurized relative to the equilibrium pressure predicted by the Gibbs-Thomson equation, based on the observations of dislocation punching surrounding bubbles in the HBS region [1]. During a LOCA transient, temperatures in the rod increase rapidly, leading to an increase in pressure in the gas contained within the bubbles. A phase-field model based on the Kim-Kim-Suzuki (KKS) formulation has been developed to answer two primary questions [2]. The first question was whether significant growth of the bubbles occurred as a result of the rapid pressure increase in the bubble and corresponding stress exerted on the surrounding fuel matrix. This stress may enhance the attraction of vacancies, potentially leading to an increased growth rate. The second question was to determine the pressure transients experienced in various bubbles in the HBS region. It was found that for typical conditions experienced during a LOCA, bubble size did not change significantly [2]. The pressure as a function of time was determined and passed to a phase-field fracture model to determine whether fracture occurred in the region surrounding individual bubbles.

In this section, the model described in Ref. [2] is applied to a set of simulated LOCA experiments conducted by Studsvik. The temperatures as a function of time in the periphery of the fuel, where the HBS is expected to be fully formed, were determined using BISON simulations. These temperatures were used as input to the KKS phase-field model. The phase-field model was used to determine the bubble pressure as a function of time in representative bubbles in the HBS structure, and these pressures were used to simulate fracture in Section 4. In the remainder of this Section, the procedure to determine temperatures and pressures as a function of time for the Studsvik rods is described.

The two Studsvik rods identified for analysis as part of this work were Rods 191 and 196. These two rods were chosen because Rod 191 experienced severe fine fragmentation and Rod 196 did not. The ability to predict whether or not fragmentation will occur is the first step in identifying the mechanism and cause of the fragmentation. Any discrepancies in the amount of fragmentation observed can be used to guide further multi-scale modeling efforts to improve the fragmentation model at the engineering scale.

Information regarding the experimental conditions and pre-irradiation histories of Rods 191 and 196 have been obtained through publicly available documents [3,4] and informed estimation when data is not available. Figure 3-1a illustrates the power history used to achieve the desired burnups prior to the Studsvik experiments. For Rod 191 this information was provided by EPRI and was said to be publicly known. For Rod 196, it is known that 2 cycles were used to achieve

the discharge burnup (~ 55 MWd/kgU) but the detailed history is not available. Therefore, a representative two cycle irradiation was assumed.

After the base irradiation the rodlets were refabricated and inserted into the Studsvik test train inside a hot cell. The experimental specimens are subjected to external heating at a rate of 5 °C/s to the target peak cladding temperature. This temperature was 1160 °C and 960 °C for Rods 191 and 196, respectively. Figure 3-1b illustrates the time history of the maximum temperature supplied to the cladding outer surface. This maximum occurs at the rod axial midplane. A slight axial profile on the temperature (20 K less at the ends) is assumed to induce localized ballooning. Table 3-1 provides additional information related to the two rods, required for analysis. The additional free volume corresponds to the volume outside of the rod but able to communicate directly with the plenum (i.e., the pressure lines).

Table 3-1
Manufacturing and operational characteristics of Studsvik Rods 191 and 196

	Rod 191	Rod 196
Rod Height (mm)	300	300
Pellet Stack Height (mm)	265.4	260.6
Pellet Radius (mm)	4.1	3.92
Gap Thickness (mm)	0.08	0.08
Cladding Thickness (mm)	0.57	0.57
Cladding Material	ZIRLO	ZIRLO
Upper Plenum Height (mm)	22.9	24.86
Lower Plenum Height (mm)	12.75	14.5
Fill Gas	He	He
Fill Gas Pressure (MPa)	3.45	3.45
Refabrication Pressure (MPa)	11	8.2
IFBA Coating	No	Yes

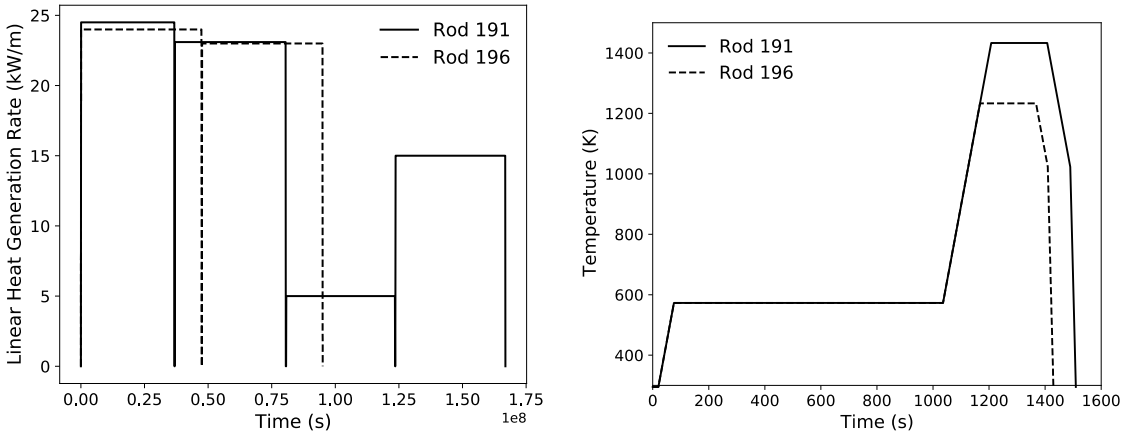

(**a**) (**b**)

Figure 3-5
(a) The linear heat generation rate supplied to the rods during base irradiation and (b) the temperature applied to the cladding outer surface during the experiment.

A 2D-RZ axisymmetric representation was used to simulate the rods using information provided in Table 3-1. For the thermal-hydraulic boundary condition during the base irradiation, the internal coolant channel model is used with an inlet pressure of 15.5 MPa, mass flow rate of 3800 kg/m^2/s, and an inlet temperature of 580 K. Many quantities of interest are tabulated by [4] for both rods including balloon characteristics and the amount of fuel that was released during the transient. In the BISON simulations, it is assumed that all fuel that has exceeded the fine fragmentation threshold has been released from the rod. Table 3-2 provides a comparison between the BISON simulations and experimental measurements for the total amount of fuel released during the LOCA. It can be seen that BISON does predict that Rod 191 will finely fragment and Rod 196 will not. However, the amount of finely fragmented fuel predicted is much lower in the BISON analysis. This is likely due to the base irradiation power history provided for Rod 191, which results in a calculated average burnup of ~67 MWd/kgU when the measured burnup at discharge was ~71 MWd/kgU. These differences in burnup can greatly influence the predictions because the pulverization threshold is directly a function of burnup and the threshold is closer to the discharge value than the calculated value.

Table 3-2
Fuel mass released during the LOCA.

BISON Rod 191 (g)	Exp. Rod 191 (g)	BISON Rod 196 (g)	Exp. Rod 196 (g)
18.6	>41	0	0

The temperature as a function of time at the edge of a representative pellet for each rod was taken from the BISON simulation, and was used as input to the KKS phase-field model described in Ref. [2]. For a detailed description of the phase-field model, please see Section 2 of Ref. [2]. For Rod 191, the temperatures at times from 1036 s to 1191 s were used as input (see Fig. 3-1(a)). (Although temperatures continued to increase beyond 1191 s, at that time significant pulverization had already occurred, so simulations were stopped at that time.) For Rod 196, the temperatures at times from 1036 s to 1368 s were used as input to the phase-field model. Simulations of the bubble size and pressure response to the temperature transients of Rod 191 and 196 were conducted for representative bubbles with varying radius, initial pressure (at fixed bubble radius), and external pressure boundary condition (at fixed bubble radius). The initial conditions for gas and vacancy compositions for each bubble were determined assuming that the pellet temperature during the rod's base irradiation (prior to refabrication for the Studsvik experiment) was 700 K. Prior to the beginning of each transient, the bubble evolution model was run, starting from a radius slightly below the nominal radius given for each simulation, to allow order parameter and concentration fields to fully equilibrate prior to the LOCA transient. The transient was initiated when the radius (as determined by the position where the bubble order parameter $\eta = 0.5$) exactly matched the nominal radius.

Simulations with varying initial gas pressure were conducted for bubbles of constant radius R = 250 nm. A gas pressure of 200 MPa is estimated to be an upper bound for the pressure of a bubble of this size, based on the dislocation punching pressure for a bubble of this size [1]. If the bubble pressure was above this value, dislocations would be punched out in the surrounding fuel

matrix, causing the bubble to grow. However, pressures could be lower than this upper bound estimate. To investigate the effect of varying initial pressure P_0, simulations with initial bubble pressures of 200, 100, and 50 MPa were conducted in Rod 191 and 196. In each case, the radius of the bubble did not change significantly during the LOCA transient. The resulting pressures are shown in Figure 3-3a and 3-3b.

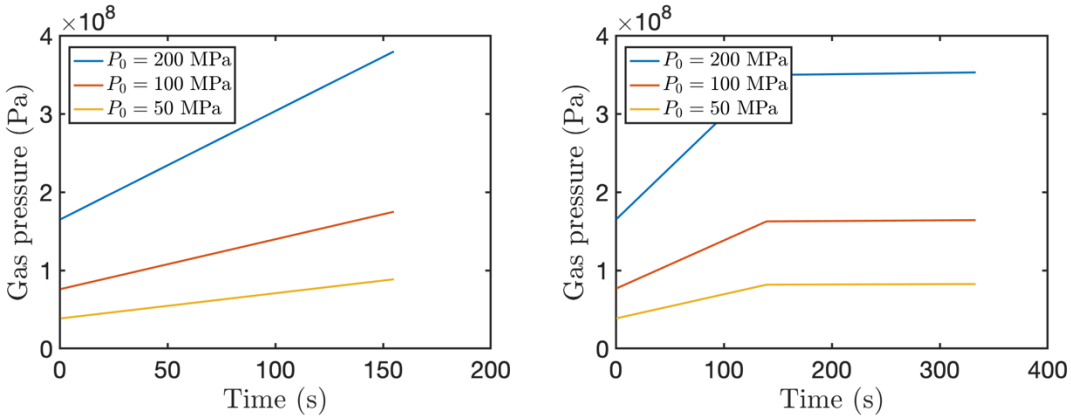

Figure 3-6
Pressure as a function of time for bubbles at the periphery of a pellet with constant *R* = 250 nm and varying initial bubble pressure P_0 for (a) Rod 191 and (b) Rod 196.

Simulations were also conducted of bubbles with varying radius. R = 250, 500, and 1000 nm were considered. The pressures for these bubbles were set at 200, 100, and 50 MPa, respectively, based on estimates from dislocation punching [1]. The pressures for these bubbles are shown in Fig. 3-4. As expected based on the previous results, the bubble radius did not change significantly during the transient, and the bubble pressure therefore increased linearly with temperature.

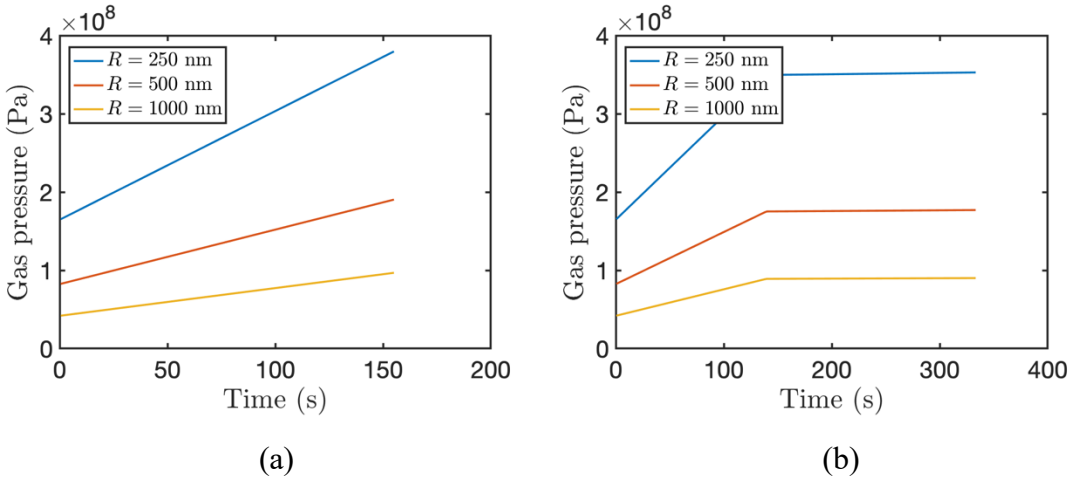

Figure 3-7
Bubble pressure as a function of time for varying bubble radius, with initial pressure determined by an upper bound estimate for (a) Rod 191 and (b) Rod 196.

Finally, the pressure at the external boundary at the edge of the domain, P_{ext}, was varied for a bubble with radius R = 500 nm. In addition to the previously simulated P_{ext} = 0, P_{ext} = 30 and 60 MPa were considered. The bubble radii again did not change significantly, and the external restraint pressure did not significantly affect the pressure transient. The external pressure may have a more significant effect on the fracture behavior in the surrounding matrix, as will be considered further in Section 4, where the pressure transients for the simulations considered in this section are passed to a phase-field fracture model to investigate fracture behavior.

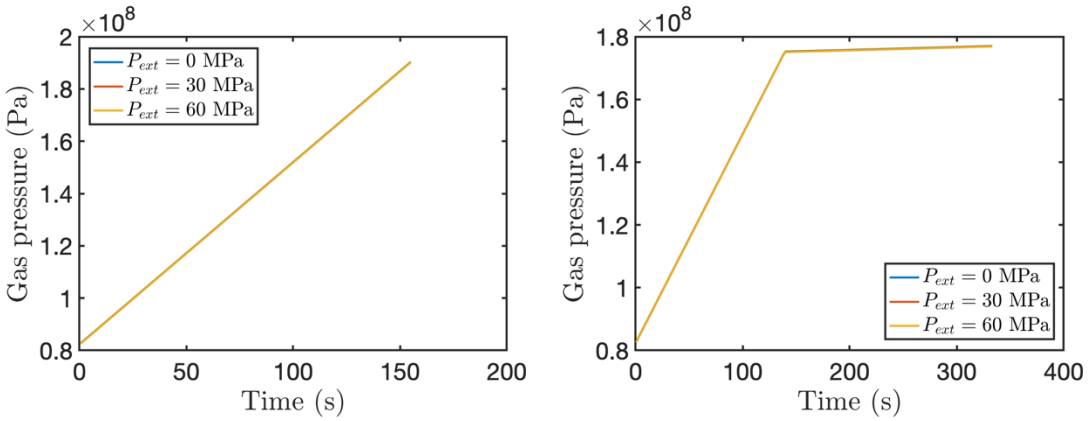

Figure 3-8
Bubble pressure as a function of time for bubbles with *R* = 500 nm, 100 MPa initial pressure, and varying external pressure P_{ext} for (a) Rod 191 and (b) Rod 196.

References

1. K. Nogita and K. Une. Irradiation-induced recrystallization in high burnup UO_2 fuel. *Journal of Nuclear Materials*, 226(3):302–310, 1995.

2. L. K. Aagesen, S. Biswas, W. Jiang, A. M. Jokisaari, D. Andersson, M. W. D. Cooper, C. Matthews. Determine fragmentation criteria in high-burnup UO_2 fuel during accident conditions. Technical report, INL/EXT-20-00558, Idaho National Laboratory, 2020.

3. M. Helin and J. Flygare. NRC LOCA tests at Studsvik, design and construction of test train device and tests with unirradiated cladding material. Technical Report, STUDSVIK/N-11/130, Studsvik, 2012.

4. M. Flanagan and P. Askeljung. Observations of fuel fragmentation, mobility and release in integral high-burnup, fueled LOCA tests. In *Enlarged Halden Program Group Meeting 2011*, 2011.

4
PHASE-FIELD FRACTURE MODELING OF HIGH BURNUP STRUCTURE FRAGMENTATION

During a LOCA transient, high-burnup fuels can fragment into very small pieces, and these small fragments could escape to the coolant when a rupture of cladding occurs. To increased burnup limits for UO_2 fuel, it is important to understand the cause of this pulverization phenomena. A rapid increase in temperature during a LOCA will cause a pressure increase in the already overpressurized bubbles in the HBS region. It has been hypothesized that intergranular fractures caused by this rapid increase in pressure lead to fine fragmentation. A new quasi-brittle phase-field fracture model is used to simulate crack initiation and propagation at large fission gas bubbles under a pressure transient. In our model, the critical fracture stress and energy release rate are completely independent of the internal length scale and their values can be determined either from experimental measurement or lower-length scale modeling. After crack initiation, the cracks will be filled with fission gas and, and our model is capable of simulating the growth of those pressurized cracks. Further details of our model can be found in [1].

We started to test whether fragmentation occurs in the fuel matrix surrounding an overpressurized bubble in the HBS region. As shown in Figure 4-1 (a), a microstructure with a size of 2.8 μm × 2.8 μm is considered. A bubble with a radius of 0.5 μm is placed at the center, which provides 10% porosity. The average grain radius is 85 nm. A uniform Young's modulus, E = 385 GPa, Poisson's ratio, ν = 0.23, and critical fracture stress, σ_c=130 MPa typical for UO2 [2,3] are used in all the simulations. To facilitate intergranular crack propagation, the critical fracture energy release G_c for grain interiors is set to be 0.0012 MPa•μm and 10 times larger than the value for grain boundaries. Symmetry boundary conditions are applied on the bottom and left sides, while top and right boundaries are traction-free. The pressure inside the bubble is monotonically increasing until crack initiation occurs. Because cracks are pressurized, crack propagation becomes unstable and cracks will grow without further increasing pressure. The maximum principal stress contour is shown in Figure 4-1 (b). The pressure inside a bubble results in a circumferential tensile stress in the matrix. When this tensile stress reaches critical fracture strength, cracks initiate at the bubble/matrix interface. After initiation, cracks propagate along grain boundaries, and reach to a free boundary. It is interesting to see that some smallest fragments have a size of individual grains.

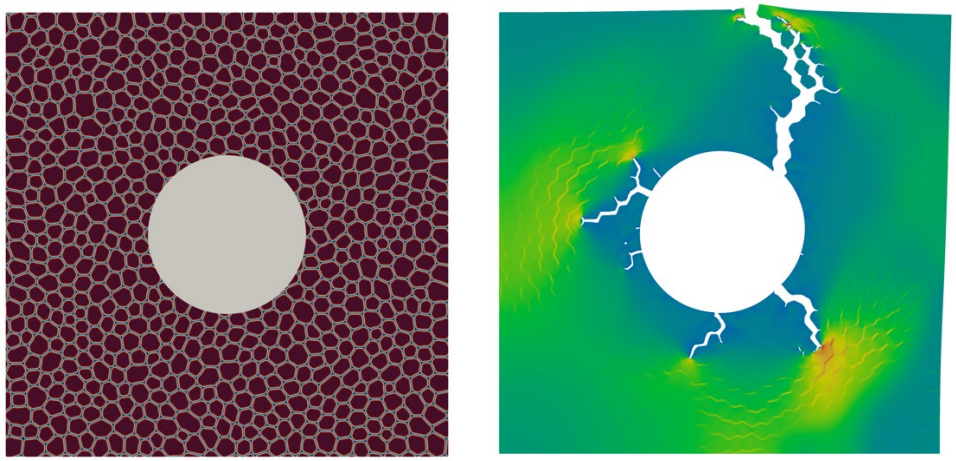

(a) **(b)**

Figure 4-1 (a) Initial microstructure configuration; (b) Cracks propagation of a pressurized bubble

In the second example, we considered two and three bubbles in the same polycrystal microstructure. The bubble radius is 0.25 μm. The centers of the two bubbles are at (0.4 μm, 1.4 μm) and (1.4 μm, 0.4 μm). The centers of the three bubbles are at (0.5 μm, 1.6 μm), (1.6 μm, 0.5 μm) and (1.6 μm, 1.6 μm). Figure 4-2 and 4-3 shows the cracks propagation and their maximum principal stress contour for the two and three bubbles case, respectively. Unlike the one bubble case where cracks propagate to a free surface, cracks propagation with multiple bubbles is strongly affected by their locations. Cracks prefers to be formed between closest bubbles. It is clear to see that those connected cracks and bubbles form a large fragment at left bottom corner in Figure 4-2 and 4-3. These fragments consist of multiple grains, and their size are determined by the bubble spatial distribution.

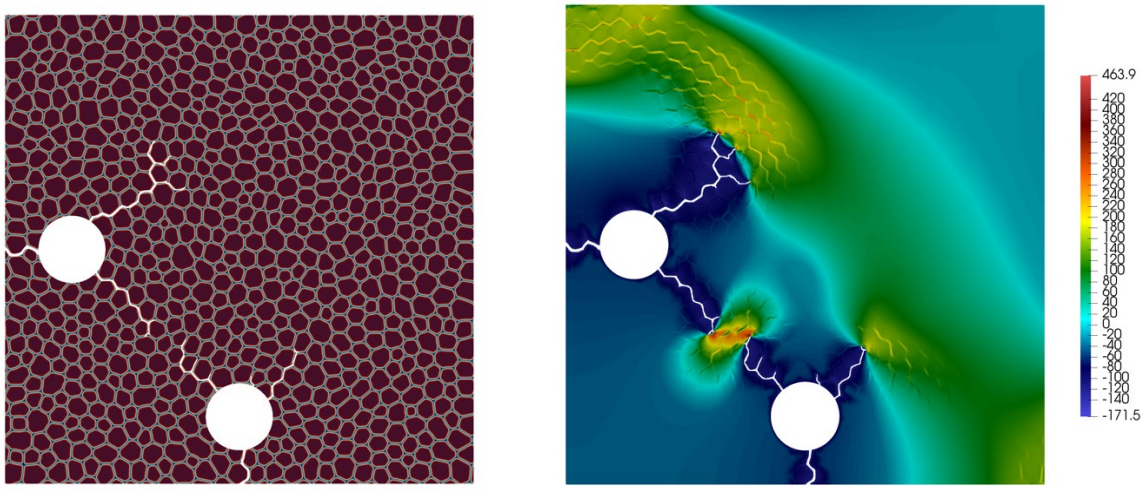

(a) **(b)**

Figure 4-2 Two bubbles case: (a) Cracks propagation; (b) Maximum principal stress

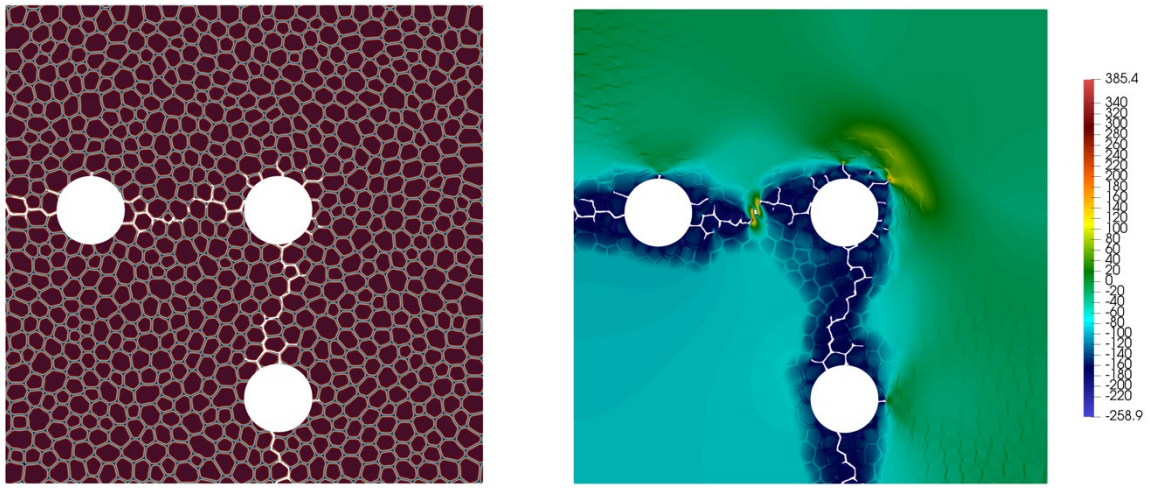

Figure 4-3 Three bubbles case: (a) Cracks propagation; (b) Maximum principal stress

In the next example, we consider bubbles with different sizes. Two radii are chosen to be 0.25 μm and 0.5 μm. The pressure inside the bubble is monotonically increasing. As shown in Figure 4-4, fracture patterns are different between these two cases. For the case with a smaller bubble, two major cracks are formed, and both propagate to outer surfaces, while for the case with a larger bubble, only one major crack is able to propagate to a free surface and the propagation of other cracks is suppressed by the major crack. Cracks initiate when tensile stress caused by the pressurized bubble reaches critical fracture strength. The critical pressures are 107.95 MPa and 88.83 MPa for the smaller and larger bubbles, respectively. The reason the critical pressure is lower for a larger bubble is that a larger bubble will cause a higher stress concentration at the bubble/matrix interface with a same pressure inside a bubble. This indicates that the bubble size will affect the fracture behavior of HBS.

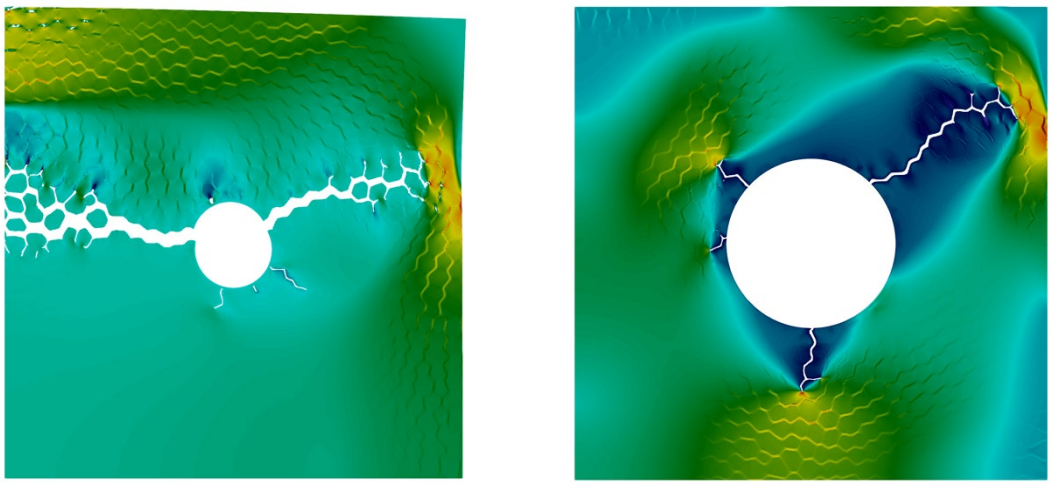

Figure 4-4 (a) Radius = 0.25 μm; (b) Radius = 0.5 μm

We next consider simulating mesoscale fractures of Rod 191 and Rod 196 under a variety of initial conditions. The pressure transient is calculated as a function of time by KKS model described in Section 3. (It should be noted that the pressures in the KKS model were calculated based on the assumed local temperature at the exterior of the rods 700K during the base irradation, while the temperature at the beginning of the Studsvik experiment was lower for both rods, so the initial pressure during the transients is lower than the nominal pressure value given.) Although different porosities were considered in the pressure calculation, the porosity does not seem to have a large impact on the pressure transient. Therefore, we did not adjust the computation domain size to provide an actual porosity. The external pressure applied on outer surfaces were set to be the same value that is used in the pressure calculation. For Rod 191 the pressure is linearly increasing, while for Rod 196 the pressure linearly increases until 150 seconds, and then remains almost unchanged. Since crack initiation occurs before the time reaches150 seconds for most of the cases considered here, the fracture behavior does not have a large difference between Rod 191 and 196. However, it should be recalled that this outcome is based on assumed values of critical fracture stress σ_c and energy release rate G_c. When a larger critical fracture stress is used, the critical pressure will become higher, and some cases for Rod 196 might predict no fracture because its pressure is no longer increasing after 150 seconds. For both cases, the critical pressure for 0.25 μm radius bubble is highest while for 1 μm radius bubble is lowest when a same external pressure was applied. The external pressure can change the critical pressure as it serves a role to compress the bubble. The critical pressure becomes significantly higher for a larger external pressure value. In a fuel pellet, such external pressure could be caused by the fuel-cladding mechanical interaction. The fracture does not occur for the case (c) in both Figure 4-5 and 4-6 because the maximum pressure does not exceed the critical pressure. For case (b), because the initial pressure value already reaches the critical value, crack initiation starts at the beginning of the simulation, and a greater number of cracks are formed to dissipate strain energy. Based on these observations, we conclude that the bubble radius, initial gas pressure and external pressure would have a large impact on the HBS fracture behavior.

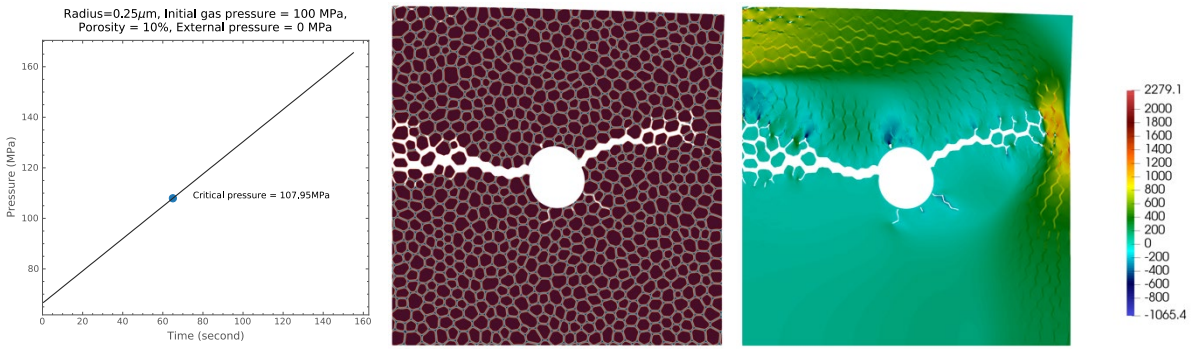

(a) Radius = 0.25 mm, initial gas pressure = 100 MPa, Porosity = 10%, External pressure = 0 MPa

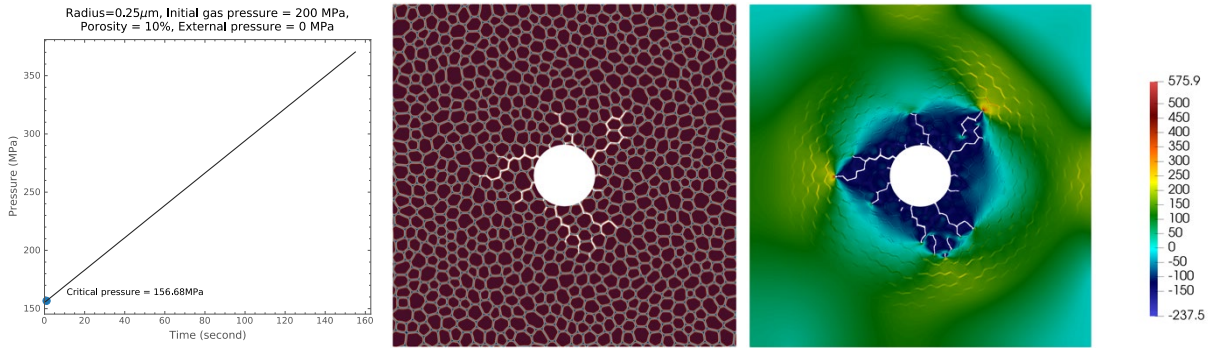

(b) Radius = 0.25 mm, initial gas pressure = 200 MPa, Porosity = 10%, External pressure = 0 MPa

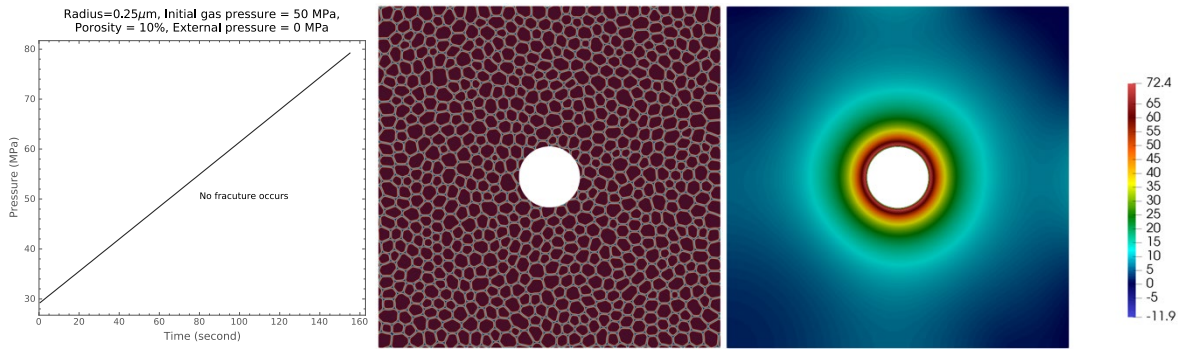

(c) Radius = 0.25 mm, initial gas pressure = 50 MPa, Porosity = 10%, External pressure = 0 MPa

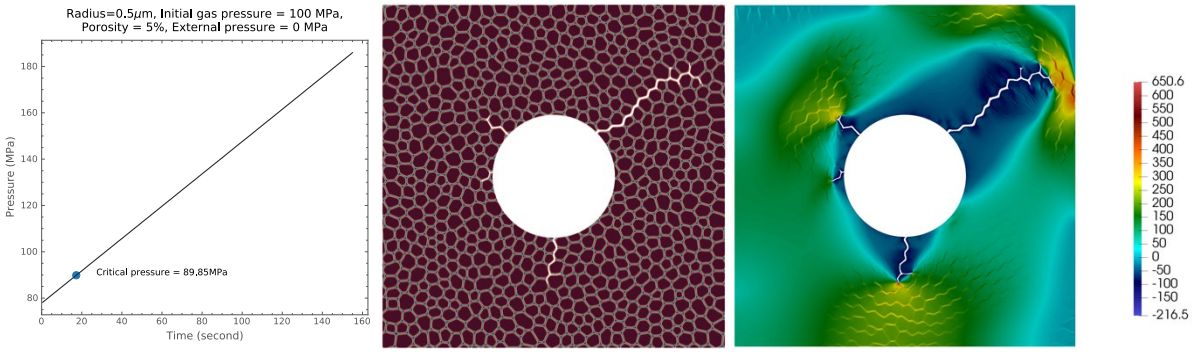

(d) Radius = 0.5 mm, initial gas pressure = 100 MPa, Porosity = 5%, External pressure = 0 MPa

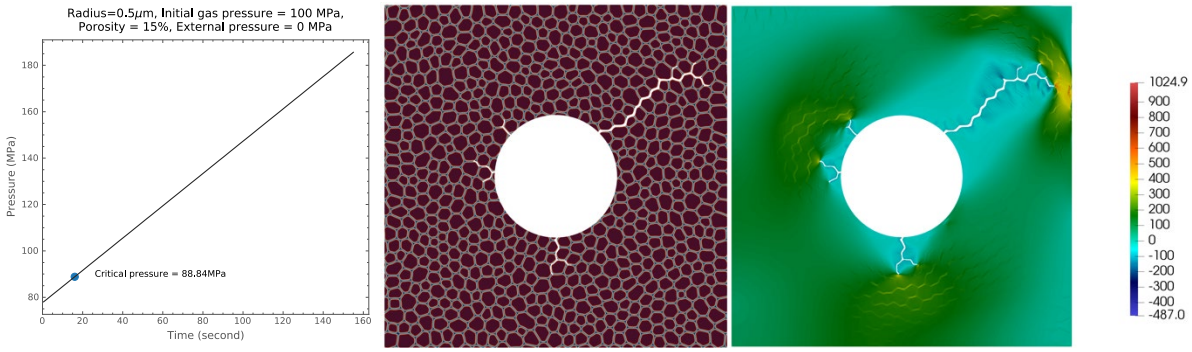

(e) Radius = 0.5 mm, initial gas pressure = 100 MPa, Porosity = 15%, External pressure = 0 MPa

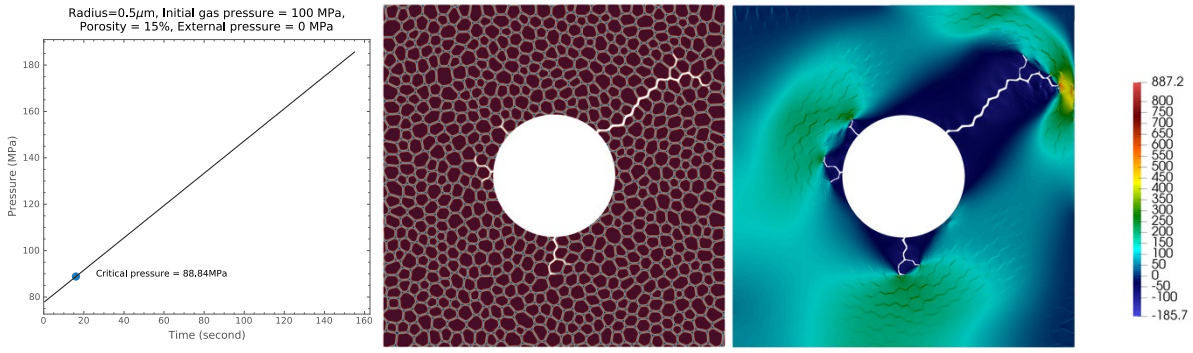

(f) Radius = 0.5 mm, initial gas pressure = 100 MPa, Porosity = 10%, External pressure = 0 MPa

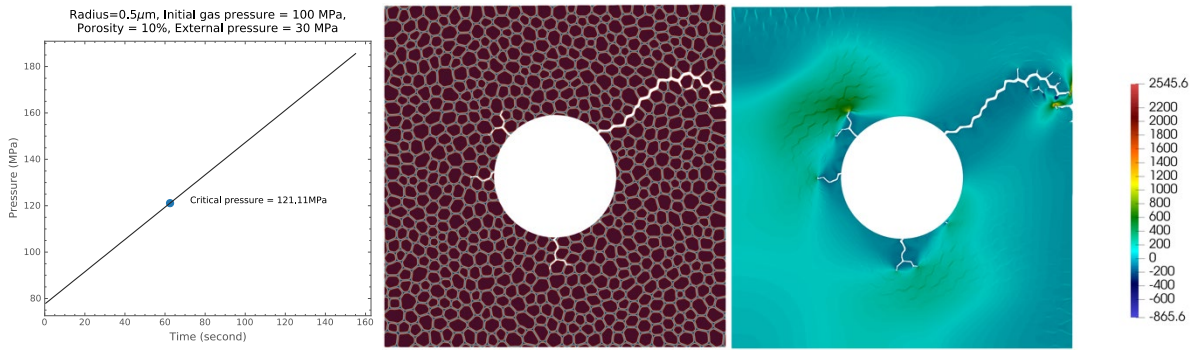

(g) Radius = 0.5 mm, initial gas pressure = 100 MPa, Porosity = 10%, External pressure = 30 MPa

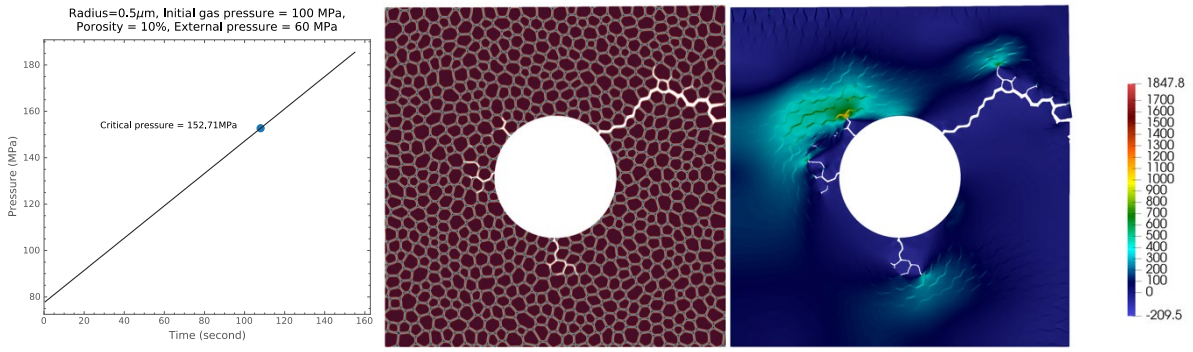

(h) Radius = 0.5 mm, initial gas pressure = 100 MPa, Porosity = 10%, External pressure = 60 MPa

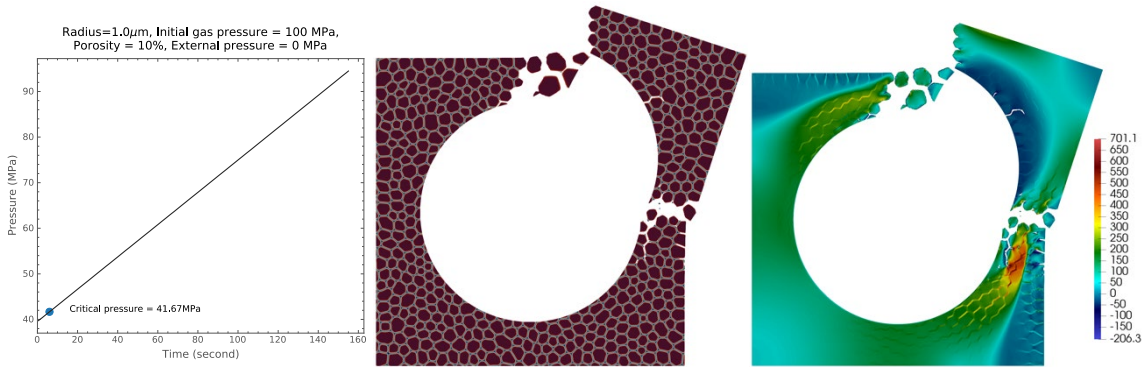

(i) Radius = 1.0 mm, initial gas pressure = 50 MPa, Porosity = 10%, External pressure = 0 MPa

Figure 4-5 Rod 191. Left column: Pressure history; Center column: Crack propagation; Right column: Maximum principal stress

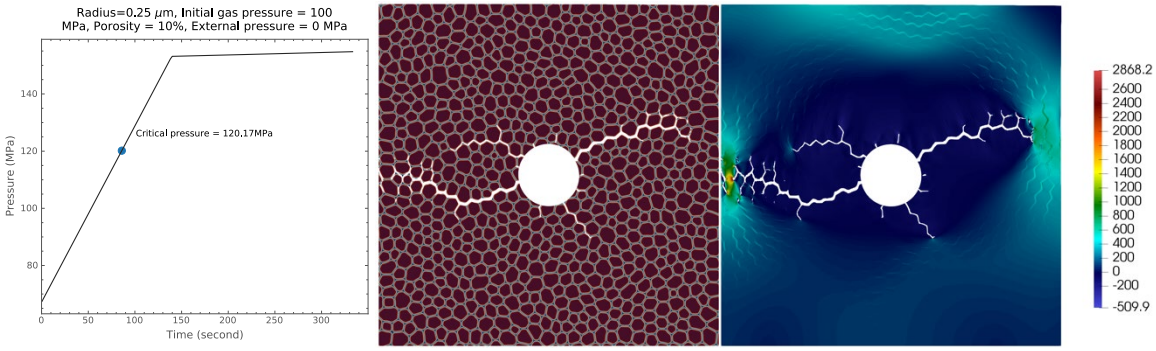

(a) Radius = 0.25 mm, initial gas pressure = 100 MPa, Porosity = 10%, External pressure = 0 MPa

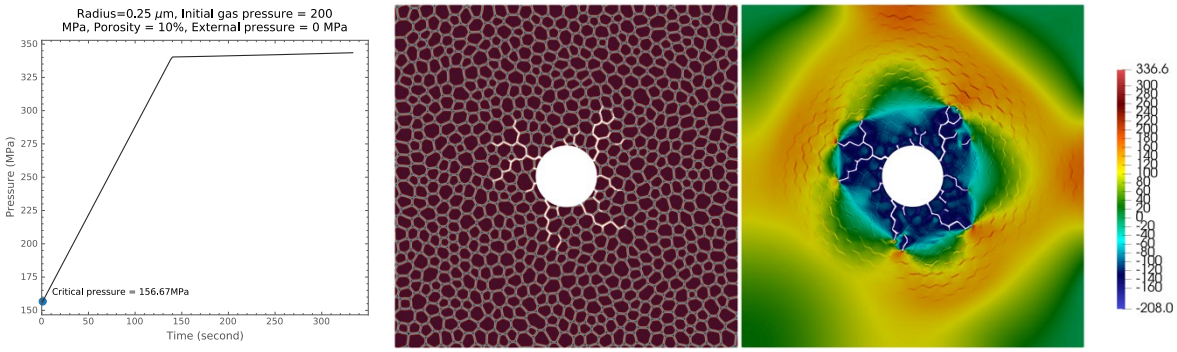

(b) Radius = 0.25 mm, initial gas pressure = 200 MPa, Porosity = 10%, External pressure = 0 MPa

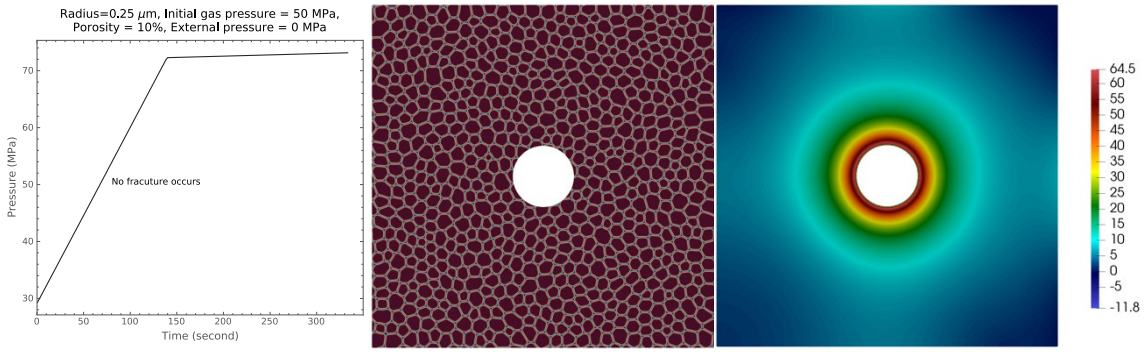

(c) Radius = 0.25 mm, initial gas pressure = 50 MPa, Porosity = 10%, External pressure = 0 MPa

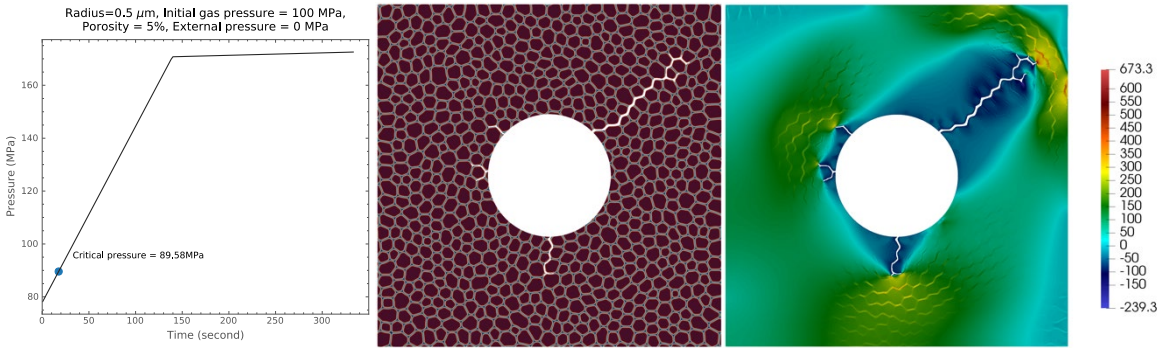

(d) Radius = 0.5 mm, initial gas pressure = 100 MPa, Porosity = 5%, External pressure = 0 MPa

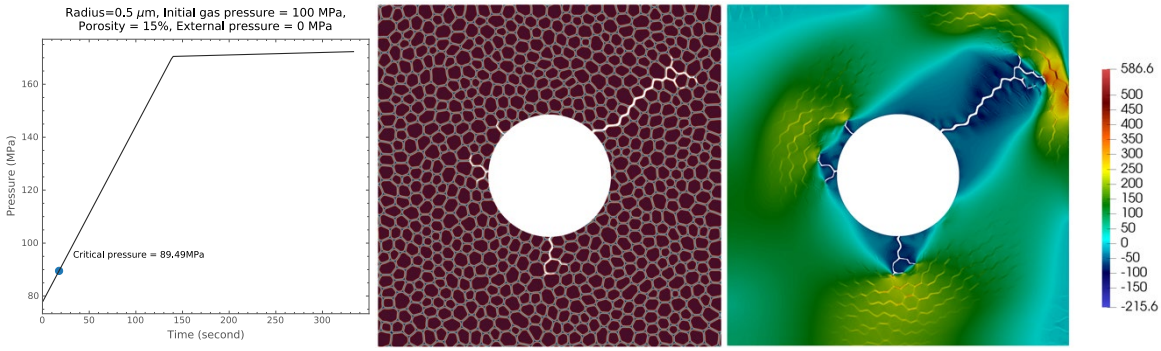

(e) Radius = 0.5 mm, initial gas pressure = 100 MPa, Porosity = 15%, External pressure = 0 MPa

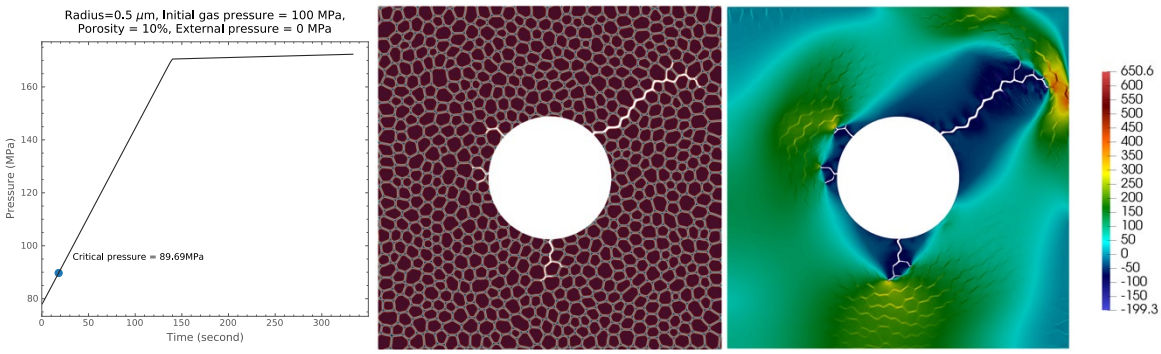

(f) Radius = 0.5 mm, initial gas pressure = 100 MPa, Porosity = 10%, External pressure = 0 MPa

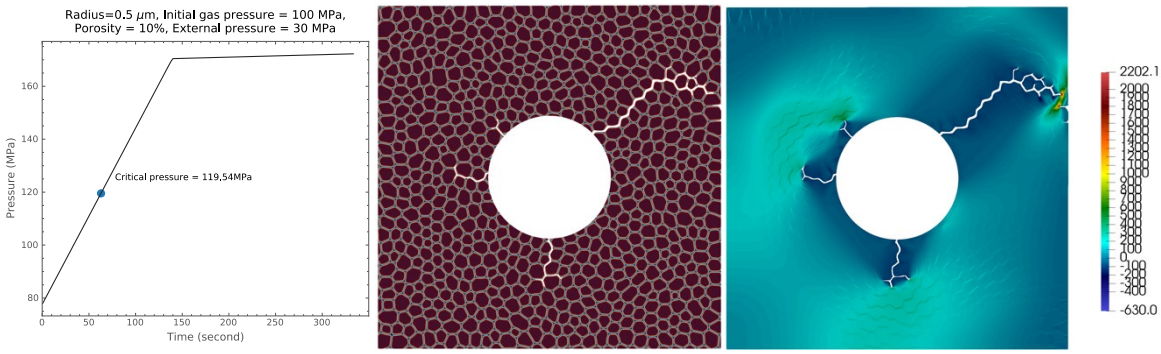

(g) Radius = 0.5 mm, initial gas pressure = 100 MPa, Porosity = 10%, External pressure = 30 MPa

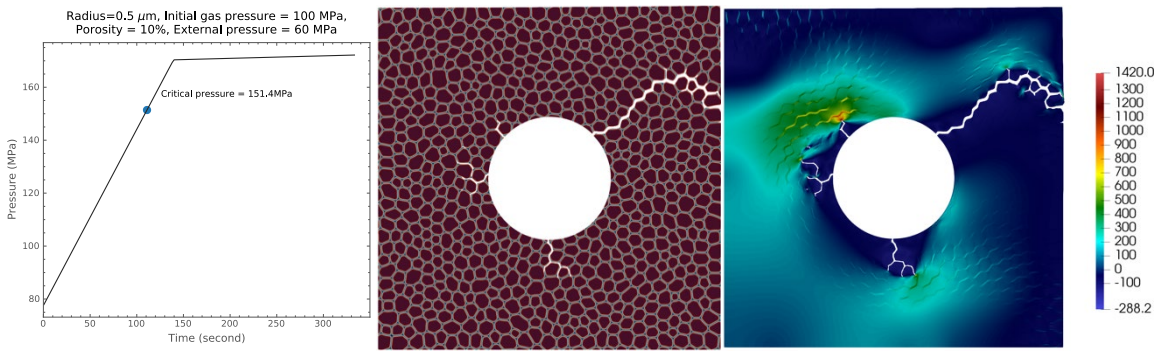

(h) Radius = 0.5 mm, initial gas pressure = 100 MPa, Porosity = 10%, External pressure = 60 MPa

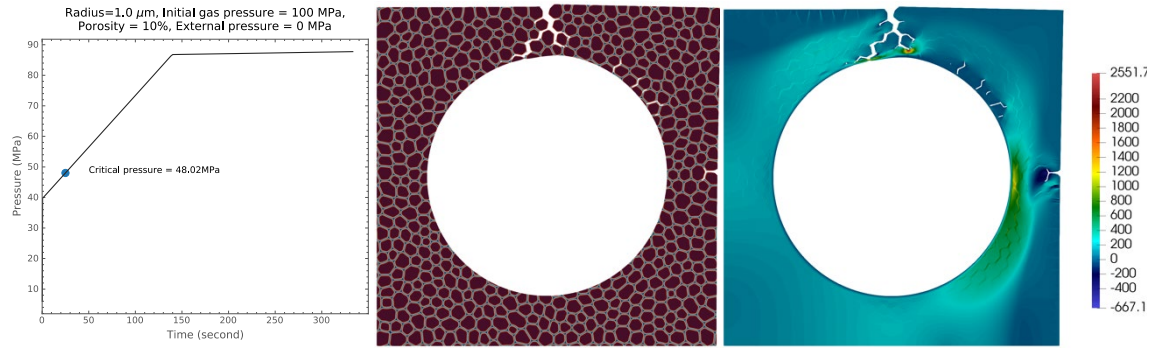

(i) Radius = 1.0 mm, initial gas pressure = 50 MPa, Porosity = 10%, External pressure = 0 MPa

Figure 4-6 Rod 196. Left column: Pressure history; Center column: Crack propagation; Right column: Maximum principal stress

We next used the simulated HBS output as our initial condition. We focused on the partial HBS, and the detailed description of the HBS simulation can be found in Section 2. Three partial HBS at different recrystallization stages were considered here. A linearly increasing pressure is applied. For all three cases, cracks initiation occurs at around 60 MPa due to their similar bubble sizes. Cracks initiation locations vary among three cases because more grains are formed around the bubble during recrystallization and their intersection points with the bubble could become possible initiation sites. In addition, the recrystallized grain structures changes grain boundary morphology, and therefore alters crack propagation directions and paths.

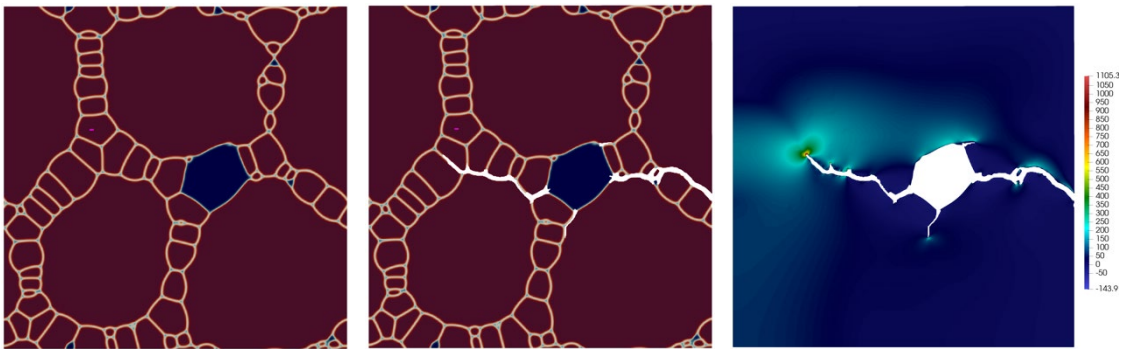

(a) Case 1

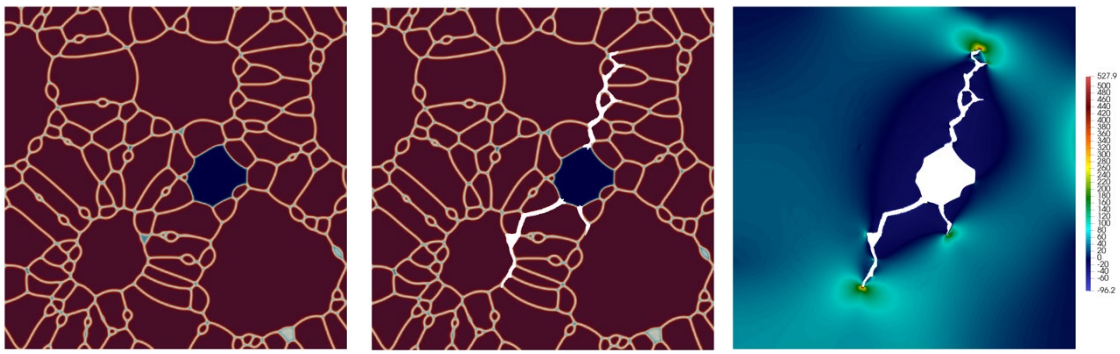

(b) Case 2

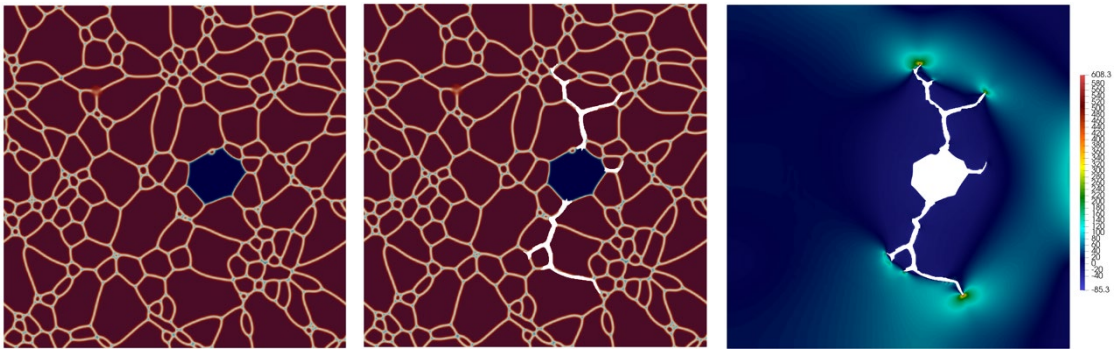

(c) Case 3

Figure 4-7 Partial HBS. Left column: Initial configuration; Center column: Crack propagation; Right column: Maximum principal stress

In the last example, we investigated the effect of bubble pressure on the critical fracture stress. The critical fracture stress can be used as an input for BISON's engineering scale fragmentation modeling. We used a fixed pressure inside a bubble, and applied an increasing displacement loading on top and right surface. The pressure values used in our simulation are 0 MPa, 20 MPa, 40 MPa, 60 MPa, 80 MPa and 100 MPa. The final configurations are shown in Figure 4-8. Because of the biaxial tensile loading, cracks propagate in two perpendicular directions. The load-displacement curve is shown in Figure 4-9. As bubble pressure is increasing, the critical fracture stress decreases and crack initiation occurs with smaller external tensile stress. This also indicates the important role of the pressure in the HBS fragmentation.

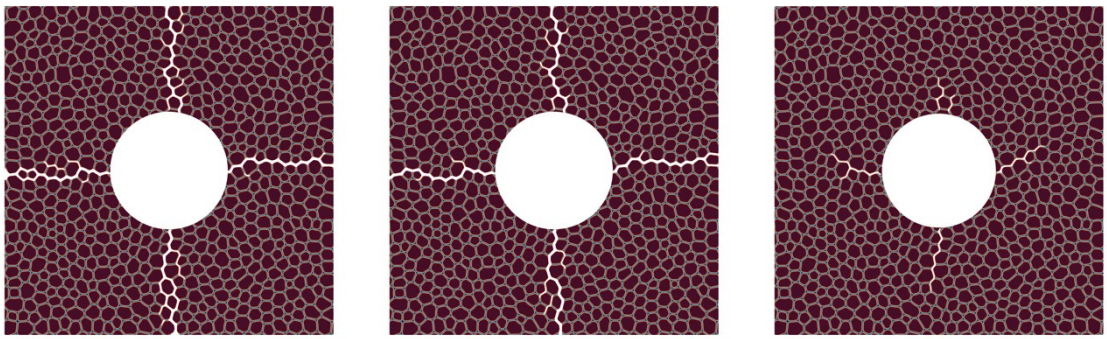

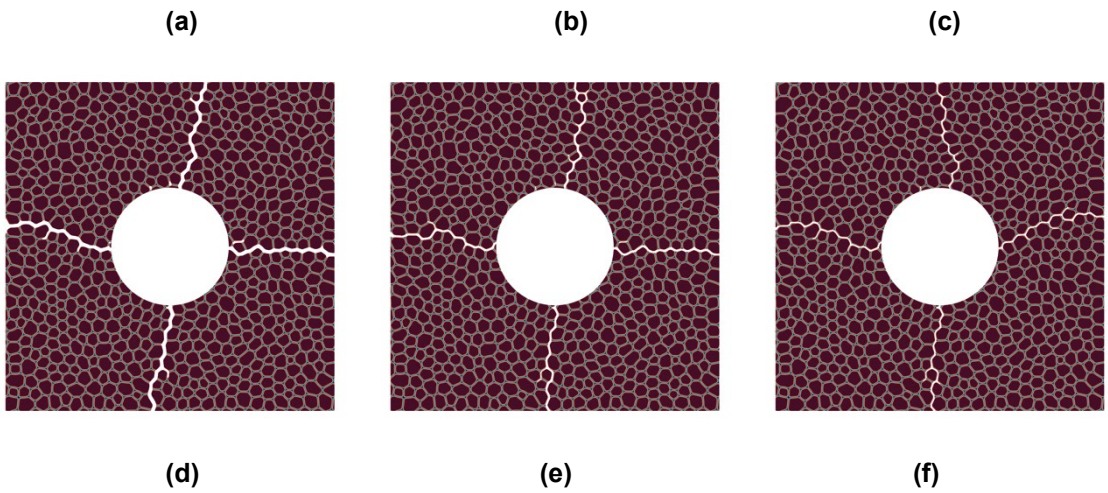

Figure 4-8 Crack propagation: (a) Pressure = 0 MPa; (b) Pressure = 20 MPa; (c) Pressure = 40 MPa; (d) Pressure = 60 MPa; (e) Pressure = 80 MPa; (f) Pressure = 100 MPa.

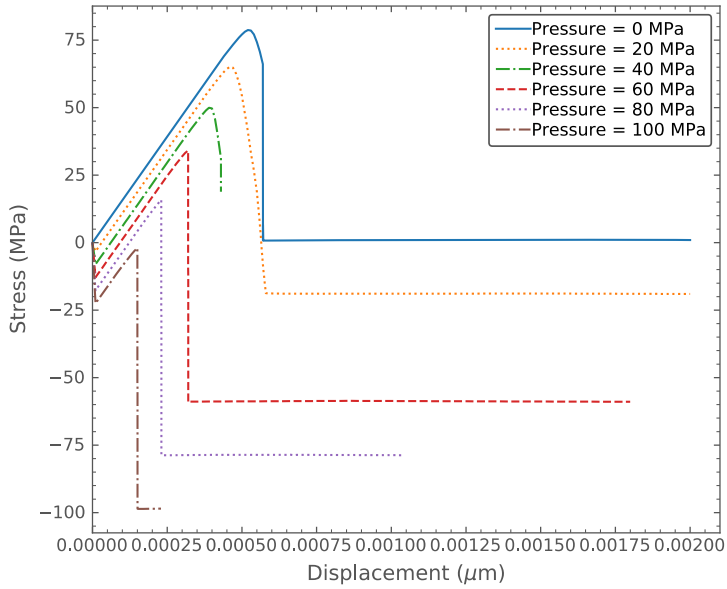

Figure 4-9 Load-displacement curve

In this section, we demonstrated that our phase field fracture model is capable of modeling of fine fragmentation phenomena and providing insights towards understanding the mechanisms of the HBS fine fragmentation. We confirmed that the pressurized bubble could cause crack initiation and propagation. The size of the bubble and external pressure will change the critical pressure for crack initiation. Our simulation showed that many fragments are formed via intergranular fracture due to pressurized bubbles. Small fragments have a size of individual grains. Large ones can form by connecting multiple bubbles via crack propagations. We also simulated crack propagation on a partial HBS at different recrystallization stages. The recrystallization changes grain structures, and therefore alters crack propagation paths and directions. Finally, we investigate mesoscale fracture behaviors of Rod 191 and 196 under a variety of initial conditions. We concluded that the bubble radius, initial gas pressure and external pressure would have a large impact on the HBS fracture behavior. Our current simulations do not show a significant different in fracture behavior between Rod 191 and 196. The discrepancies between our simulation and experiments can be addressed in the future by (1) using better values of fracture strength and G_c that are obtained from LANL's

lower length scale modeling and INL MFC's experimental measurements; (2) incorporating reasonable boundary conditions into our fracture modeling from BISON's engineering scale modeling; (3) using more realistic HBS microstructures that are simulated by our phase-field HBS model.

References

1. L. K. Aagesen, S. Biswas, W. Jiang, A. M. Jokisaari, D. Andersson, M. W. D. Cooper, C. Matthews. Determine fragmentation criteria in high-burnup UO_2 fuel during accident conditions. Technical report, INL/EXT-20-00558, Idaho National Laboratory, 2020.

2. K. Govers, Comparison of interatomic potentials for UO_2, Journal of Nuclear Materials, 2014

3. W. Jiang, B. W. Spencer, J. E. Dolbow, Ceramic nuclear fuel fracture modeling with the extended finite element method, Engineering Fracture Mechanics, 2020